chemistry

MDPI

Article

Solid Phase Nitrosylation of Enantiomeric Cobalt(II) Complexes

Mads Sondrup Møller, Morten Czochara Liljedahl, Vickie McKee and Christine J. McKenzie *

Department of Physics, Chemistry and Pharmacy, University of Southern Denmark, Campusvej 55, 5230 Odense M, Denmark; madssm@sdu.dk (M.S.M.); mlilj18@student.sdu.dk (M.C.L.); mckee@sdu.dk (V.M.)
* Correspondence: mckenzie@sdu.dk

Abstract: Accompanied by a change in color from red to black, the enantiomorphic phases of the cobalt complexes of a chiral salen ligand (L^{2-}, Co(L)·CS_2, and Co(L) (L = $L^{S,S}$ or $L^{R,R}$)) chemisorb NO (g) at atmospheric pressure and rt over hours for the CS_2 solvated phase, and within seconds for the desolvated phase. NO is installed as an axial nitrosyl ligand. Aligned but unconnected voids in the CS_2 desorbed Co($L^{R,R}$)·CS_2 structure indicate conduits for the directional desorption of CS_2 and reversible sorption of NO, which occur without loss of crystallinity. Vibrational circular dichroism (VCD) spectra have been recorded for both hands of LH_2, Zn(L), Co(L)·CS_2, Co(L), Co(NO)(L), and Co(NO)(L)·CS_2, revealing significant differences between the solution-state and solid-state spectra. Chiral induction enables the detection of the ν_{NO} band in both condensed states, and surprisingly also the achiral lattice solvent (CS_2 (ν_{CS} at 1514 cm^{-1})) in the solid-state VCD. Solution-state spectra of the paramagnetic Co(II) complex shows a nearly 10-fold enhancement and more extensive inversion of polarity of the vibrations of dominant VCD bands compared to the spectra of the diamagnetic compounds. This enhancement is less pronounced when there are fewer polarity inversions in the solid state VCD spectra.

Keywords: chirality; vibrational circular dichroism; solid–gas reaction; chemisorption; nitrosyl

Citation: Møller, M.S.; Liljedahl, M.C.; McKee, V.; McKenzie, C.J. Solid Phase Nitrosylation of Enantiomeric Cobalt(II) Complexes. *Chemistry* **2021**, *3*, 585–597. https://doi.org/10.3390/chemistry3020041

Academic Editors: Catherine Housecroft and Katharina M. Fromm

Received: 31 March 2021
Accepted: 26 April 2021
Published: 28 April 2021

1. Introduction

NO is biologically important, but also a highly toxic gas, and materials for its sorptive removal from exhausts are of great interest. A number of diverse materials, from metal oxides, zeolites, and metal-organic frameworks have shown the ability to selectively sorb NO, in some cases reversibly [1–6]. Chemisorptive processes can result in the transformation of the sorbed NO into less toxic compounds and precedence for this was demonstrated recently using the crystalline solid-state of a dicobalt(II) complex, which co-chemisorbs NO and O_2. Accompanied by metal oxidation, their conversion to a coordinated nitrite and nitrate counter anion ensues through a series of unidentified in-crystal reactions [7].

We were interested in investigating the chemisorptive reactivity of NO by an isolated mononuclear Co(II) site inside the crystalline lattice of a molecular solid in efforts to understand the mechanism of the host–guest, solid–gas chemistry of the aforementioned molecular dicobalt(II) complexes [7]. In particular, we wanted to investigate whether the in-crystal conversion of NO and O_2 to NO_2^- and NO_3^- is dependent on the presence of two closely-located cobalt ions working cooperatively to activate these guest substrates. Mononuclear Co(salen) has been shown to react with NO in both solution- [8] and solid-states [8,9], and offers the opportunity to explore this possibility. Unfortunately, however, no details of the structural or spectroscopic changes in the solids have been reported for the solid–gas reaction. It is unknown whether or not well-defined pores to allow transport through the solid are requisite, whether or not the process is true chemisorption (where bonds are formed), whether the presumed in-solid NO coordination to Co(II) results in its oxidation, and whether the reaction is reversible. We have, therefore, reinvestigated the NO gas–solid reaction for the salen system, however, the parent scaffold has been replaced with *N*,*N*′-bis(3,5-di-t-butylsalicylidene)-1,2-cyclohexanediamine (L^{2-}), the derivative used

in the manganese(III) chloride complex that is also known as 'Jacobsen's catalyst' [10], and is used for catalyzing asymmetric epoxidation reactions [10–12]. A survey of the Cambridge structural database [13] of the crystal structures of metal complexes of L^{2-} suggests that the peripheral bulky tert-butyl groups of L^{2-} ensure that mononuclear Co sites are isolated from each other by preventing the formation of crystal phases containing dimeric $(M(salen))_2$ [14–18], which form when a phenolato oxygen atom of each salen on adjacent complexes bridge between the two metal ions. Another advantage is that, unlike some phases of the parent Co(salen) and its derivatives, Co(L) does not bind O_2.

Another aspect of this work is the fact that L^{2-} provides chirality by virtue of the aliphatic backbone carbon atoms to give $L^{S,S}$ and $L^{R,R}$ (Scheme 1). With respect to the use of L^{2-} for constructing enantiopure complexes to catalyze asymmetric reactions, we wished also to learn whether a chiral ligand would induce chirality into an achiral axial co-ligand, since this is a proxy for a bound substrate.

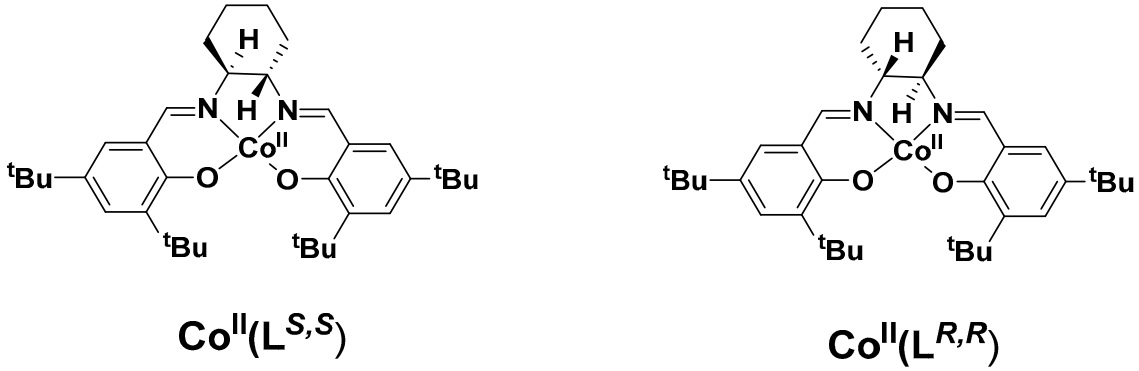

Scheme 1. *S*,*S* and *R*,*R* conformations of $Co^{II}(L^{S,S})$ and $Co^{II}(L^{R,R})$.

2. Materials and Methods

Caution NO is a highly toxic gas. CS_2 vapors are also toxic.

2.1. Instrumentation

Mass spectra are recorded with electrospray ionization (ESI) on a Bruker micrOTOF-Q II spectrometer (nanospray, capillary temperature = 180 °C, spray voltage = 3.7 kV). UV-vis spectra were recorded on an Agilent 8453 spectrophotometer in 1 cm quartz cuvettes. VCD and IR spectra were recorded on a CHIRALIR-2X^{TM} spectrometer equipped with a single PEM, a resolution of 4 cm^{-1}, optimized at 1400 cm^{-1}, and in a single block with 50000 scans. All VCD spectra are baseline corrected by half differentiating from the other enantiomer, i.e., subtracting the VCD spectrum of one enantiomer from that of the other enantiomer and dividing the intensity of the resulting spectrum by two, and vice versa. All solution state VCD spectra were recorded in $CDCl_3$ using an ICLSL-4 liquid cell with BaF_2 windows and a path length of 75 µm. Solutions were prepared by dissolving 30 mg sample in 0.3 mL $CDCl_3$. All solid phase VCD spectra were recorded as mulls applied between two circular BaF_2 windows (Ø25 mm × 4 mm), and the sample holder was rotated at a constant speed throughout the recording to reduce artifacts. Mulls were prepared by grinding, with an agate mortar and pestle, 20 mg sample with 50 µL Nujol oil. Powder X-ray diffraction data were collected on a Synergy, Dualflex, AtlasS2 diffractometer using CuKα radiation (λ = 1.54184 Å) and the CrysAlis PRO 1.171.40.67a suite [19]. Powdered samples were adhered to the mounting loop using Fomblin®Y, and diffractograms were recorded with a detector distance of 120 mm, using Gandolfi scans with a single kappa setting, and an exposure time of 200 s.

2.2. Single Crystal X-ray Diffraction

The crystals used for Single Crystal X-ray Diffraction (SCXRD) were taken directly from the mother liquor and mounted using Fomblin®Y to adhere the crystal to the mount-

ing loop. X-ray crystal diffraction data were collected at 100(2) K on a Synergy, Dualflex, AtlasS2 diffractometer using CuKα radiation (λ = 1.54184 Å) and the CrysAlis PRO 1.171.40.67a suite [19], and corrected for Lorentz-polarization effects and absorption. Using SHELXLE [20], the structure was solved by dual space methods (SHELXT [21]) and refined on F^2 using all the reflections (SHELXL-2018 [22]). All the non-hydrogen atoms were refined using anisotropic atomic displacement parameters, and hydrogen atoms were inserted at calculated positions using a riding model. Parameters for data collection and refinement are summarized in Table 1. The chirality in these complexes is provided by the cyclohexane ring in the ligand backbone, however, the remainder of the structures, including the heavier cobalt and (for Co($L^{R,R}$)·CS_2 and Co(NO)($L^{R,R}$)·CS_2) sulfur atoms, are arranged almost centrosymmetrically. As a result, the $|E^2 - 1|$ statistics, cumulative intensity distribution plots, and Wilson plots (SI Figures S6–S8) appear to favor a centrosymmetric structure (as does the initial estimate of the Flack x parameter in SHELXT for Co(NO)($L^{R,R}$)·CS_2), and Platon ADDSYM in checkCIF suggests a (pseudo) center of symmetry may be present. Nevertheless, all three structures were successfully refined in the chiral space group $P2_1$, showing the expected chair conformation of the cyclohexane rings, all with *R*,*R* chirality. When carbon disulfide is desorbed from Co($L^{R,R}$)·CS_2 to produce Co($L^{R,R}$), the crystal quality is reduced slightly, resulting in weak high angle data. The structure of Co($L^{R,R}$), therefore, contains more uncertainties.

2.3. Computational Details

The VCD and IR calculations considered in this work were performed using (unrestricted) density functional theory (DFT) calculations performed using Jaguar [23] through the Maestro graphical interface. [24] All structures have been geometry optimized in isolation using B3LYP/LACVP** [25,26], and vibrational frequencies have also been calculated at this level of theory. All calculations are solution gas phase calculations. For $L^{R,R}H_2$, different conformations were calculated using the OPLS2005 [27] forcefield, and the VCD and IR spectra were based on a Boltzmann average of these conformations. For Zn($L^{R,R}$), the VCD and IR spectra are based on only the most stable conformation.

2.4. Synthesis

The *R*,*R* and *S*,*S* enantiomers of *N*,*N*′-bis(3,5-di-t-butylsalicylidene)-1,2-cyclohexanediamine, $L^{R,R}H_2$ and $L^{S,S}H_2$, were prepared according to literature methods with a reported ee. of >95% [28]. The *R*,*R* and *S*,*S* enantiomers of *N*,*N*′-bis(3,5-di-tert-butylsalicylidene)-1,2-cyclohexanediaminozinc(II) (Zn($L^{R,R}$) and Zn($L^{S,S}$)) [29] and *N*,*N*′-bis(3,5-di-tert-butylsalicylidene)-1,2-cyclohexanediaminocobalt(II) (Co(L^{RR}) and Co(L^{SS})) [30] were also synthesized according to literature procedure. All other chemicals were purchased from Sigma-Aldrich and were used without further purification.

2.4.1. Co($L^{R,R}$)·CS_2 and Co($L^{S,S}$)·CS_2

A degassed solution of Co(L^{RR}) or Co(L^{SS}) (0.250 g) in CS_2:*n*-hexane (16 mL, 1:1 *v*/*v*) was placed in a vial which was then placed inside a large glass jar with an air tight lid, and the solution was allowed to slowly evaporate at 5 °C in the fridge, yielding ruby red block crystals suitable for single crystal X-ray diffraction. Yield 0.227 g, 80.6%.

IR (Nujol) cm^{-1}: 1609 (m, C=C), 1591 (m, C=N), 1524 (vs, C=S), 1254 (m, C–O).

ESI-MS (pos. mode, MeCN): found (calcd) m/z = 603.217 (603.34, [Co(LR,R)]+, $C_{36}H_{52}CoN_2O_2$ 100%).

2.4.2. Co($L^{R,R}$) and Co($L^{S,S}$) (Desolvated from Co($L^{R,R}$)·CS_2 and Co($L^{S,S}$)·CS_2)

A sample of Co($L^{R,R}$)·CS_2 or Co($L^{S,S}$)·CS_2 (0.25 g, size 0.05–1 mm^3) was placed inside a 10 mL round bottom flask, and the flask was attached to a rotary evaporator. The crystals were heated to 95 °C in vacuo (~10^{-2} mbar) and rotated for one hour, resulting in a color change from translucent dark red to opaque red/orange. Co($L^{R,R}$) and Co($L^{S,S}$) were isolated in a quantitative yield.

IR (Nujol) cm^{-1}: 1608 (s, C=C), 1596 (vs, C=N), 1524 (m, C=N), 1255 (m, C–O).

ESI-MS (pos. mode, MeCN): found (calcd) m/z = 603.217 (603.34, $[Co(L^{R,R})]^+$, $C_{36}H_{52}CoN_2O_2$ 100%).

UV-vis (DCM) λ_{max}/nm (ε/M^{-1} cm^{-1}): 247 (36,012), 428 (11,446).

2.4.3. Co(NO)($L^{R,R}$) and Co(NO)($L^{S,S}$)

Crystals of Co($L^{R,R}$) or Co($L^{S,S}$) (0.25 g, size 0.05–1 mm^3) were placed in a Schlenk tube (30 mL), and the Schlenk line was evacuated and filled with N_2 (3 cycles). NO (1.2 bar) was then admitted into the system, resulting in a color change from opaque red/orange to opaque black within seconds, and the closed tube was then allowed to stand for one hour. Before opening to air, the system was evacuated and flushed with N_2 (3 cycles). Co(NO)($L^{R,R}$) and Co(NO)($L^{S,S}$) were isolated in a quantitative yield. Recrystallization of Co(NO)($L^{R,R}$) (0.25 g) from CS_2:*n*-hexane (8 mL, 1:1 *v*/*v*) via the same procedure as described above for Co($L^{R,R}$)·CS_2 yielded black needle crystals of Co(NO)($L^{R,R}$)·CS_2 suitable for single crystal X-ray diffraction.

IR (Nujol) cm^{-1}: 1659 (w, N=O) 1638 (vs, C=N), 1608 (s, C=C,), 1524 (w, C=N), 1255 (w, C–O).

ESI-MS (pos. mode, MeCN): found (calcd) m/z = 603.317 (603.34, $[Co(L^{R,R})]^+$, $C_{36}H_{52}CoN_2O_2$, 100%), 634.320 (634.34, $[Co(NO)(L^{R,R})H]^+$, $C_{36}H_{53}CoN_3O_3$, 4.98%)

UV-vis (DCM) λ_{max}/nm (ε/M^{-1} cm^{-1}): 267 (18,040), 366 (5391).

3. Results and Discussion

3.1. Reaction of Solid-State Co(II) Complexes with NO

Two new enantiomorphic phases of Co(L) (L = $L^{S,S}$, $L^{R,R}$) have been prepared and structurally characterized. Co(L)·CS_2, was obtained by recrystallization of Co(L) from CS_2/*n*-hexane. A strong band in the IR spectrum at 1524 cm^{-1} is associated with the ν_{CS} of co-crystallized CS_2. This band is very close to that for free CS_2 at 1520 cm^{-1}, indicating little interaction with the cobalt atom. Co(L)·CS_2 undergoes CS_2 loss on heating at 95 °C for 1 h at 10^{-2} mbar to reproduce Co(L), however it is now a new unreported phase that is different to the starting phase. Both Co(L)·CS_2 and Co(L) react in the solid state with NO gas (1 atm, rt, unground crystals ranging in size from 0.05 to 1 mm^3) (Scheme 2).

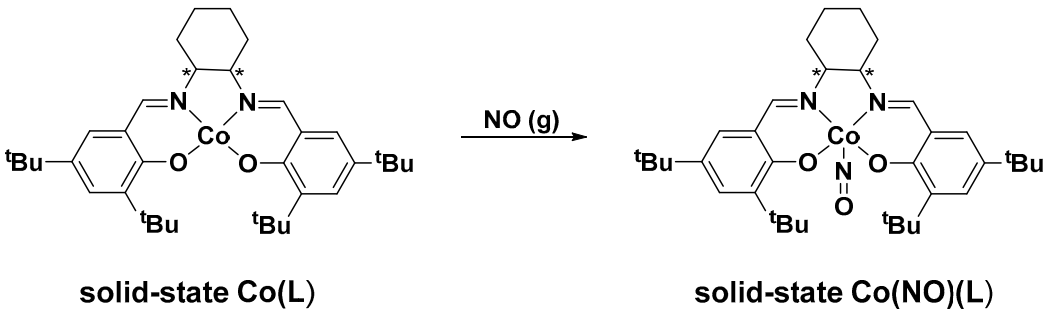

Scheme 2. Preparation of Co(NO)(L) from Co(L) by a solid-state gas reaction with NO (1 atm).

This reaction is accompanied by a color change from red to black (Figure 1, SI film), with the process occurring over several hours for the CS_2 solvate and in seconds to minutes for the desolvated phase, depending on sample size. Co(NO)(L) is formed inside the lattice. The IR spectrum of the product shows a low intensity ν_{NO} band at 1657 cm^{-1}.

The NO can be removed stoichiometrically from Co(NO)(L) by heating to 195 °C. This process has been cycled three times without significant decomposition (Figure 2). Powder X-ray diffraction (PXRD) shows that crystallinity is retained after CS_2 desorption, NO chemisorption, and subsequent desorption without significant change to the pattern (Figure 3). The pattern for the recrystallized sample of the nitrosyl complex is also similar. These suggest that that the packing is similar throughout these sequential gas (CS_2/NO)–solid sorption/chemisorption and desorption processes.

Figure 1. Crystals of (**a**) Co(L)·CS_2; (**b**) Co(L), obtained by the desorption of CS_2 from Co(L)·CS_2; and (**c**) Co(NO)(L) after the NO gas–solid reaction with Co(L).

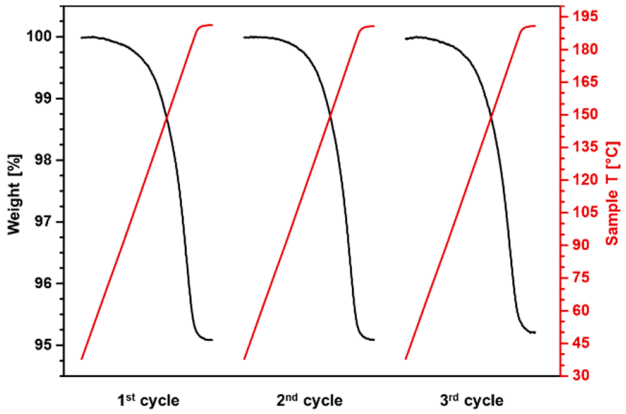

Figure 2. Thermogravimetric analysis showing reversible and ostensibly stoichiometric binding of NO to Co(L) to give Co(NO)(L) over three cycles. The red lines are the heating profile, while the black lines are the weight loss profile.

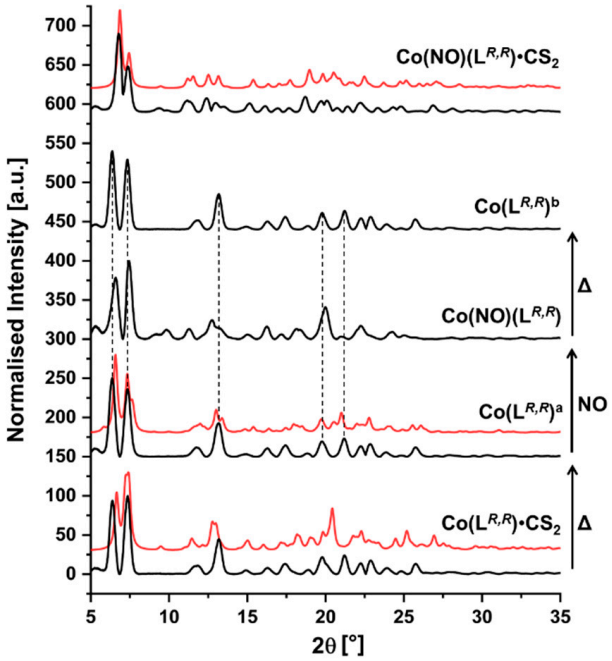

Figure 3. Series of PXRD patterns for an enantiomorphic phase of the CS_2 solvate, before and after desorption of CS_2, followed by the product of NO chemisorption and subsequent NO desorption. Top pattern is of recrystallized Co(NO)(L) as a CS_2 solvate. Note: Black—measured; red—calculated from single crystal structural data.

3.2. Structures of Enantiomorphic Phases

Single crystal X-ray structures were obtained for Co($L^{R,R}$)·CS_2, Co($L^{R,R}$) and Co(NO)($L^{R,R}$)·CS_2. Notably, the data for Co($L^{R,R}$) were obtained from a crystal of Co($L^{R,R}$)·CS_2 after desorption of the CS_2, which occurs in a single crystal-to-single crystal (SCSC) transformation for many of the individual crystals, i.e., many of the crystals do not break but retain their morphology in the process. This is not the case for the subsequent NO sorption, where the crystals break into smaller pieces and no crystal of adequate quality for a structure determination by SCXRD was found. PXRD establishes, however, that crystallinity is retained. Recrystallization of the solid Co(NO)($L^{R,R}$) (from CS_2/*n*-hexane) was necessary for obtaining a single crystal X-ray structure of the cobalt nitrosyl. Details of the data collections are provided in Table 1. Solid state iron porphyrin complexes have been shown to be capable of NO gas sorption, in this case the process occurs in an SCSC transformation [31,32].

Table 1. Selected crystallographic data for Co($L^{R,R}$)·CS_2, Co($L^{R,R}$), and Co(NO)($L^{R,R}$)·CS_2. All data obtained using Cu K_α radiation.

Compound	**Co($L^{R,R}$)·CS_2**	**Co($L^{R,R}$)**	**Co(NO)($L^{R,R}$)·CS_2**
Empirical formula	$C_{37}H_{52}N_2O_2S_2Co$	$C_{36}H_{52}N_2O_2Co$	$C_{37}H_{52}N_3O_3S_2Co$
Formula weight	679.85	603.72	709.86
Temperature/K	100.00(10)	100.00(10)	100.00(10)
Crystal system	monoclinic	monoclinic	monoclinic
Space group	$P2_1$	$P2_1$	$P2_1$
a [Å]	13.55410(10)	26.2740(4)	14.12020(10)
b [Å]	9.96900(10)	9.5866(2)	10.02300(10)
c [Å]	26.59490(10)	29.2826(4)	25.9282(2)
α [°]	90	90	90
β [°]	92.1290(10)	113.379(2)	95.5600(10)
γ [°]	90	90	90
Volume [$Å^3$]	3591.04(5)	6770.1(2)	3652.27(5)
Z	4	8	4
μ [mm^{-1}]	5.085	4.210	5.052
Tmin/Tmax	0.499/0.958	0.688/1.000	0.183/1.000
$(\sin\theta/\lambda)_{max}$	0.749	0.684	0.698
Final R1, wR2 indexes [$I \geq 2\sigma(I)$]	0.0250, 0.0638	0.0952, 0.1822	0.0292, 0.0757
Final R1, wR2 indexes [all data]	0.0267, 0.0649	0.1113, 0.1898	0.0346, 0.0801
Flack parameter [33]	−0.0189(11)	0.082(4)	−0.019(2)
Goof on F^2	1.022	1.198	1.013
Peak/hole [e $Å^{-3}$]	0.28/−0.30	0.58/−0.84	0.42/−0.27
CCDC Numbers	2073657	2073658	2073659

The structures of Co($L^{R,R}$)·CS_2 and Co(NO)($L^{R,R}$)·CS_2 are shown in Figure 4. That of Co($L^{R,R}$) is similar (SI Figure S1). The cobalt ion in Co($L^{R,R}$)·CS_2 is close to square planar, with the cobalt atom lying 0.023 Å above the O–N–N–O plane of L^{2-}. The sum of angles around the Co(II) is 360.11°, with cis angles of between 86.73° and 94.02°. The average Co–O_{salen} and Co–N_{salen} bond distances are 1.844(2) Å and 1.861(2) Å, respectively. The cyclohexane backbones show the expected chair conformation of the *R,R* enantiomer. The metric parameters for the unsolvated phase of Co($L^{R,R}$) are similar (Table 2).

The bond lengths and angles for the nitrosyl complex are comparable to those found for its homologue Co(NO)(salen) [34], with the geometry around the cobalt atom being close to square pyramidal. The angles deviate an average of 4.9° from 90°, and the cobalt atom lies even further (0.237 Å) above the O–N–N–O plane of L^{2-} compared to the Co(II) complexes, with no significant interaction to the cobalt ion in the other axial position. The distances and the associated angles are very similar to the cobalt(II) complexes, however, the flat chelating salen ligand can be expected to impose constraints. Analysis of the O/N–Co distances in other cobalt complexes of L^{2-} (SI Figure S2) show that it is typical for

square pyramidal Co(III) complexes to display similar values to the Co(II) square planar complexes. Nitrosyl is a well-known non-innocent ligand, and has been assigned formally to the extremes of NO^+, $NO^{\cdot}$ and NO^-. The N–O distance in free radical NO is 1.15 Å, and in Co(NO)($L^{R,R}$)·CS_2 it is less than 0.03 Å greater. With various structural ambiguities, we describe the nitrosyl complex using the Enemark-Feltham notation [35], i.e., $\{Co(NO)\}^8$.

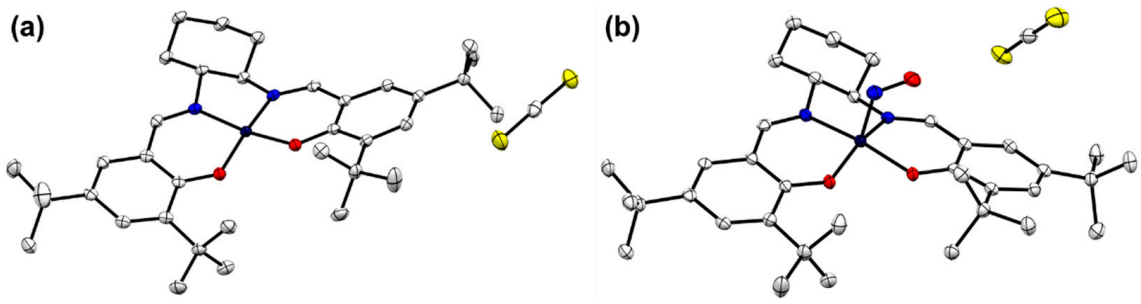

Figure 4. Single crystal X-ray structures of (**a**) Co($L^{R,R}$)·CS_2, and (**b**) Co(NO)($L^{R,R}$)·CS_2. Atom colors: red—oxygen; blue—nitrogen; white—carbon; yellow—sulfur; dark blue—cobalt. Atomic displacement ellipsoids are drawn at 50% probability and hydrogen atoms are omitted for clarity.

Table 2. Selected mean bond distances and angles.

Compound	Co($L^{R,R}$)·CS_2	Co($L^{R,R}$)	Co(NO)($L^{R,R}$)·CS_2
Co–N [Å]	1.861(2)	1.861(9)	1.894(3)
Co–O [Å]	1.844(2)	1.847(8)	1.877(2)
∠O–Co–O [°]	86.93(7)	87.3(3)	84.34(9)
∠N–Co–N [°]	86.54(9)	86.9(4)	85.42(11)
∠N–Co–O [°]	93.78(8)	93.5(4)	93.60(10)
Co–NO [Å]	-	-	1.818(3)
CoN=O [Å]	-	-	1.179(3)
∠Co–N=O [°]	-	-	122.0(2)

The packing in the three structurally characterized compounds show layers of the complexes in a herringbone arrangement, where the tert-butyl groups para to the phenolato O atom reside in columns parallel to the *a* axis (Figure 5, SI Figures S3 and S4). In the solvates, the co-crystallized CS_2 molecules are also located in these columns. Desorption of CS_2 from Co($L^{R,R}$)·(CS_2), to give Co($L^{R,R}$), results in a relatively large unit cell change with approximate doubling of the *a* axis from 13.55410(10) Å to 26.2740(4) Å, and an increase in the β-angle from 92.1290(10)° to 113.379(2)°. The packing in Co($L^{R,R}$) is shown in Figure 5. The voids occur where the CS_2 occupied the lattice of Co($L^{R,R}$)·(CS_2). They are not connected and have an approximate size of 216.34 $Å^3$ (3.2% of unit cell volume). The kinetic diameters of CS_2 and NO are approximately 3.6 Å and 3.17 Å, respectively [36], and, on the basis of the structures and the approximate void diameter of 7.4 Å, it is tempting to posit that the exit of CS_2 will be synchronously accompanied by rotation about the C–C bond attaching the tert-butyl groups to the aryl ring. The chemisorption of NO occurs with small shifts in the PXRD pattern (Figure 3), suggesting this unit cell is changed slightly but with related packing. The recrystallized Co(NO)($L^{R,R}$)·CS_2 shows a marginally (1.7%) expanded unit cell compared to that of Co($L^{R,R}$)·CS_2. The two most intense diffraction peaks in the PXRD of Co(NO)($L^{R,R}$) are moved towards a slightly higher 2θ angle upon chemisorption of NO compared to the parent phase Co($L^{R,R}$), which corresponds to a change in the interplanar distance (d) from 13.8962 Å and 12.0268 Å in Co($L^{R,R}$) to 13.4325 Å and 11.8659 Å in Co(NO)($L^{R,R}$) (Figure 3). This can be attributed to a slight molecular rearrangement, in order to make room for binding of NO at the cobalt atom.

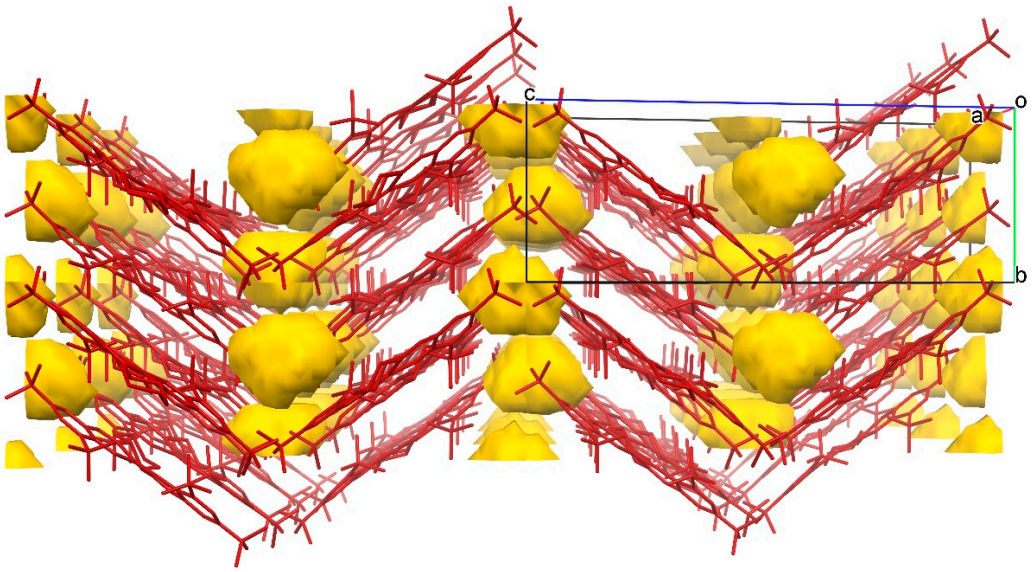

Figure 5. Packing diagram for Co($L^{R,R}$) with voids in yellow (1.2 Å probe radius and 0.7 Å grid spacing). Hydrogen atoms are omitted for clarity.

3.3. Solution-State Vibrational Circular Dichroism (VCD) Spectra

VCD allows the characterization of enantiopure compounds through the analysis of IR-active bands. The primary quantity associated with IR absorbance is the dipole strength, however, VCD measures the differential absorbance ($\Delta A(\nu) = A_{left}(\nu) - A_{right}(\nu)$) that is proportional to the rotational strength; a quantity which depends both on the electric and magnetic dipole transition moments. Thus, the VCD intensities are not directly correlated with the intensities in the IR spectrum. VCD has predominantly been used to analyze solution and pure liquid phases of organic molecules. In this work, VCD spectra for both hands of LH_2 and the Zn(II), Co(II), and Co(III)NO complexes of L^{2-} have been recorded. The IR spectra (purple) and the corresponding VCD spectra for the $L^{S,S}$- and $L^{R,R}$-based systems (colored blue and red respectively) are shown in Figure 6. The IR spectra show that the band due to the salen $\nu_{C=N}$, the most intense in the IR spectra, shifts from 1632 cm^{-1} in LH_2 to a lower frequency (1598 cm^{-1}) in coordination with Zn^{2+} in accordance with the decrease in the C=N bond order as a consequence of co-ordinate bond formation by the azomethine nitrogen lone pair. The band due to the $\nu_{C=N}$, is the most intense in the VCD spectrum of the Zn(II) complexes. Despite being the most intense in the IR spectrum for $L^{S,S}H_2$ and $L^{R,R}H_2$, this is now a relatively moderate signal in the VCD spectra of $L^{S,S}H_2$ and $L^{R,R}H_2$, where, instead, several unassignable C–C and C–H vibrations are the most intense. Computational analysis to aid in the assignment of bands in VCD spectra is common in the study of enantiopure organic compounds, and we have performed such an analysis with reasonable success for $L^{R,R}$ and Zn($L^{R,R}$) (SI Figure S5). The introduction of transition metal ions makes calculation a formidable task, perhaps even impossible for the paramagnetic complexes. In this work, we take a fingerprint approach to the characterization. The fact that we have characterized both enantiomers and achieved consistently opposite band polarities demonstrates the reliability of the results.

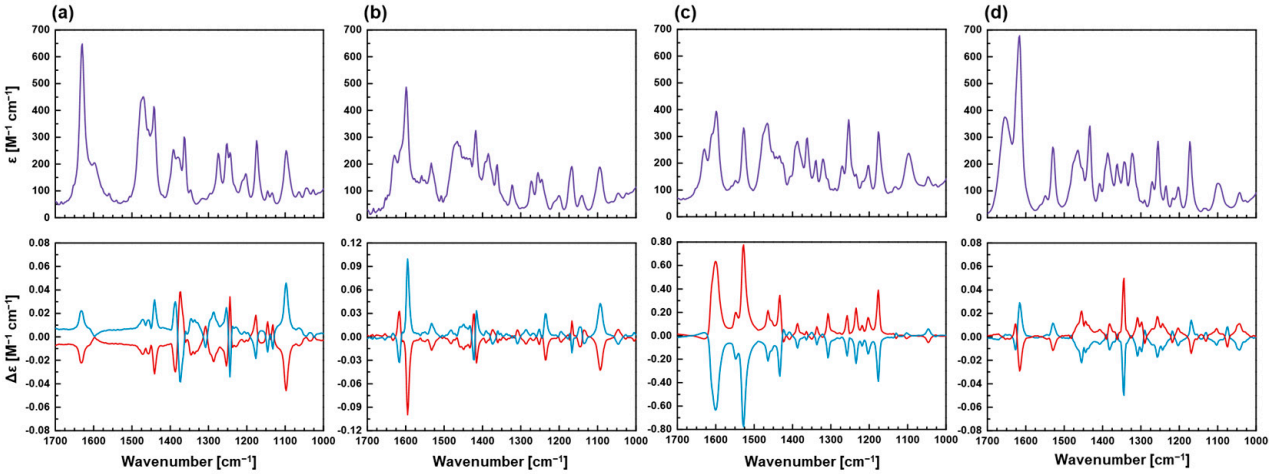

Figure 6. Solution ($CDCl_3$) IR (top, purple line, obtained using equimolar concentrations of both hands) and VCD (bottom) spectra of (**a**) $L^{S,S}H_2$ and $L^{R,R}H_2$, (**b**) Zn($L^{S,S}$) and Zn($L^{R,R}$), (**c**) Co($L^{S,S}$) and Co($L^{R,R}$), and (**d**) Co(NO)($L^{S,S}$) and Co(NO)($L^{R,R}$). The $L^{S,S}$- and $L^{R,R}$-based systems are colored blue and red, respectively.

An increase in VCD signal strength is noticeable in the comparison of the VCD spectra of the Zn(II) complexes and those for LH_2. This arises because coordination locks the ligand into fewer conformations [37]. The VCD spectra for Co($L^{S,S}$) and Co($L^{R,R}$) are very different to those of the structurally analogous Zn(II) complexes. Apart from many different positions and relative intensities, the spectrum is close to monosignate (all bands for one hand showing one polarity). A change in the absorbance of left and right circularized IR radiation causes the polarity inversion of some bands. In addition, the signals are approximately nine times as intense as those for all the other compounds. This is associated with the diamagnetism and paramagnetism of low-lying excited electronic states in the Co(II) complexes. Electronic transitions are strongly magnetic-dipole dependent and hence, when present, can induce enhanced VCD by the coupling of the electronic magnetic-dipole transition moments with the smaller vibrational magnetic-dipole moments responsible for normal VCD intensity [37].

Azide is a linear, non-chiral ligand with a track record as a proxy vibrational spectroscopic and structural marker for O_2 binding sites. Accordingly, it binds to the iron center at the distal position of the heme group. Bormett et al. [38] have reported the VCD spectra of ferric hemoglobin azide, and show that the azide ligand somehow borrows magnetic dipole intensity from the chiral environment inherent to this protein to produce a VCD signal. The effect we see in this work is analogous, and we have used VCD to assess the chiral induction of the signals for achiral NO in the complexes of L^{2-}. This co-ligand can be regarded as a proxy substrate in a reaction catalyzed by complexes of enantiopure L^{2-}, which, particularly with respect to asymmetric catalytic synthesis, is easily accessible in both hands. Although close to the dominating salen imine ν_{CN} (1616 cm^{-1}) band in Co(NO)(L), the ν_{NO} (1657 cm^{-1}) can be distinguished in the IR spectra as the second most intense band (Figure 6d, top). Notably, a signal for ν_{NO} can also be seen at this position in the VCD spectrum, but its intensity is now very low by comparison to many other bands in the spectrum. This indicates that, while chiral induction occurs, it is not particularly strong. In this context, it is interesting to note that the enantiomeric excess in catalytic reactions with complexes of $L^{R,R}$ and $L^{S,S}$ are sometimes disappointing [39–43].

3.4. Solid State VCD Spectra

While the use of Nujol mull, KBr discs, or even neat powders in sample preparation for recording solid-state IR spectra is commonplace, irreproducibility due to a high sensitivity to inhomogeneity in particle size, especially because the technique is a transmission method, makes classic solid-state sample preparation for VCD spectroscopy less straightforward. This is probably why solid state VCD spectra are rarely reported [37]. In the context of the

molecular solid-state chemistry described here, it was interesting for us to develop this technique. We found that, with consistent grinding and Nujol, it was possible to obtain reproducible spectra. The solid-state IR and VCD spectra of Co(L)·CS_2 and Co(L) are shown in Figure 7a,b. In contrast to the IR spectra, the VCD spectra of the two phases are easily distinguishable. Obviously, this is information that was lost in the solution state. The differences between the solution-state and solid-state spectra are greater in the VCD spectra compared to the IR spectra: There is far less tendency towards a monosignate spectra for both phases in the solid-state spectra. Fascinatingly, an n_{CS} signal related to co-crystallized CS_2 is visible in VCD spectrum at 1514 cm^{-1} (Figure 7a). This indicates supramolecular chiral induction of this achiral molecule. The signal disappears on CS_2 desorption to form Co(L) (Figure 7b). The intensity of the IR band at 1524 cm^{-1} also decreases. This band comprises an overlap of the n_{CS} with a band that does not appear in the VCD spectrum.

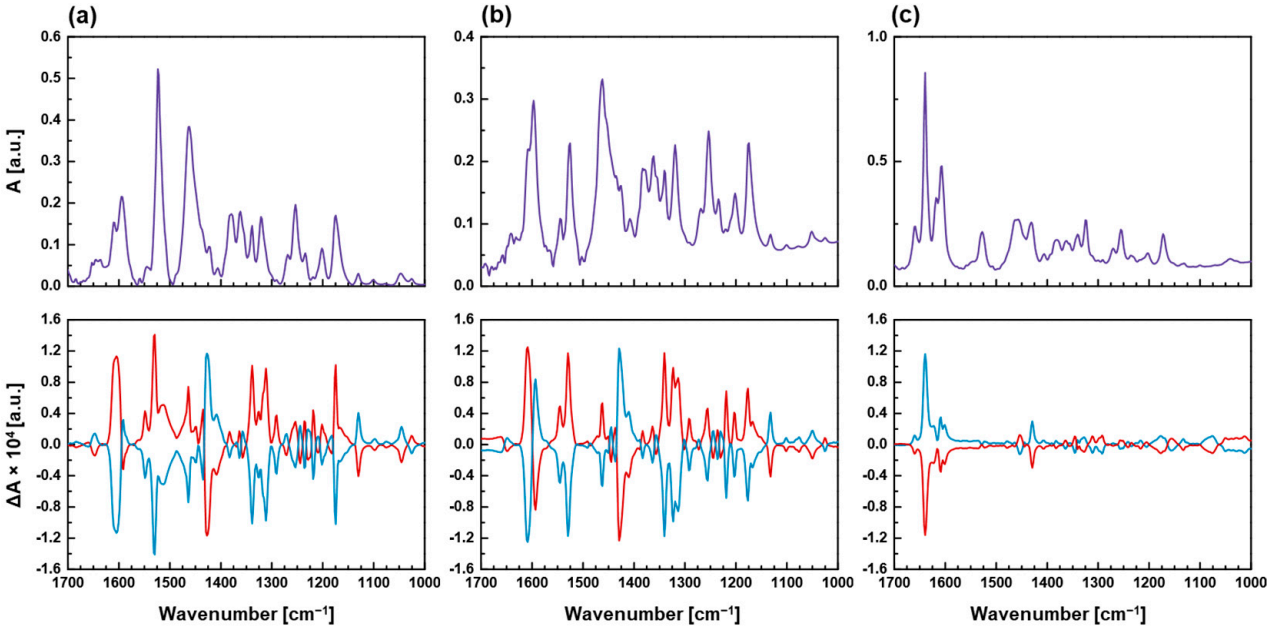

Figure 7. Solid-state IR spectra of a mixture of equal amounts of both hands of the complexes (purple line) and solid-state VCD spectra of (**a**) Co(L)·CS_2, (**b**) Co(L), and (**c**) Co(L)(NO) (blue line complexes of $L^{S,S}$; red line complexes of $L^{R,R}$).

The solid-state IR and VCD spectra of Co(NO)(L) are shown in Figure 7c. It is difficult to assign the bands in the spectra, however, the band at 1638 cm^{-1}, assigned to the imine ν_{CN}, is significantly more intense than all the others. It also shows an increase of 22 cm^{-1} compared to the band assigned to this vibration in the solution state spectra of the same complex. This suggests a change in the electronics of the complex due to different supramolecular interactions in the solution-state versus the solid-state. The higher wavenumber for ν_{CN} suggests that this bond is stronger in the solid state. Indirectly, this suggests that the NO is a stronger donor to the Co atom in the solid-state. The well-resolved, but low intensity, band at 1659 cm^{-1} is assigned to ν_{NO}. There is significant polarity inversion between comparable signals in the paramagnetic Co(II) compounds, the diamagnetic $\{Co(NO)\}^8$ phase, and the $\{Co(NO)\}^8$ systems in the solution and solid states. Curiously, an unassigned band at 1344 cm^{-1}, which is most intense in the solution-state spectrum of Co(NO)(L), appears to be absent in the solid-state VCD spectrum.

4. Conclusions

We have demonstrated chemisorption of NO into an ostensibly non-porous crystalline material, but postulate that transient conduits for CS_2 desorption and NO chemisorption form because the tert-butyl groups can rotate around the bond between the aryl and the tert-butyl carbon atoms. The gas–solid reactions involved in the transitions between

$Co(L)\cdot CS_2$, Co(L), and Co(L)(NO) occur in crystal to crystal transformations, and in one case an SCSC transformation. The NO binds reversibly, and the materials do not allow O_2 to react with the bound NO. This supports the hypothesis that the in-crystal reactivity seen for the crystalline dicobalt(II) complexes described in the introduction, where sorbed NO and O_2 were transformed to a nitrite ligand and a nitrate counter anion [7], is dependent on two cobalt(II) ions in close proximity. Accessibility and the specific coordination sphere and geometry, however, also clearly play important roles.

The crystalline solid state offers advantages beyond the solution state, through the provision of tailored cavities that might amplify chirality compared to the solution state. This study shows that in-crystal chemistry for the first time, with the induction of chirality onto both a chemisorbed achiral guest and a physisorbed co-crystallized achiral guest. Crystal phases themselves can occur in chiral space groups without being constructed from enantiopure molecules. Both situations offer feasibility for absolute asymmetric synthesis (AAS) [44] inside solid states. The rare use of VCD spectroscopy to characterize the complexes in this work illustrates its untapped potential in the study of enantiomers of metal coordination complexes in both solution- and solid-states.

Supplementary Materials: The following are available online at https://www.mdpi.com/article/10.3390/chemistry3020041/s1. CCDC 2073657–2073659 contain the supplementary crystallographic data for this paper. These data can be obtained free of charge from The Cambridge Crystallographic Data Centre via www.ccdc.cam.ac.uk/structures.

Author Contributions: M.S.M. synthesized the compounds, performed calculations, and prepared the first manuscript draft; M.S.M. and M.C.L. performed measurements, processed and analyzed the data, and designed the figures; V.M. assisted with X-ray crystallography; C.J.M. conceived and supervised the work. All authors reviewed and edited the manuscript. All authors have read and agreed to the published version of the manuscript.

Funding: The work was supported by the Danish Council for Independent Research (Grant 9041-00170B) and the Carlsberg Foundation grant CF15-0675 for the X-ray diffractometer.

Institutional Review Board Statement: Not applicable.

Informed Consent Statement: Not applicable.

Data Availability Statement: The data presented in this study are available in supplementary material.

Conflicts of Interest: The authors declare no conflict of interest.

References

1. Zhang, W.X.; Yahiro, H.; Mizuno, N.; Izumi, J.; Iwamoto, M. Removal of nitrogen monoxide on copper ion-exchanged zeolites by pressure swing adsorption. *Langmuir* **1993**, *9*, 2337–2343. [CrossRef]
2. Xiao, B.; Byrne, P.J.; Wheatley, P.S.; Wragg, D.S.; Zhao, X.; Fletcher, A.J.; Thomas, K.M.; Peters, L.; Evans, J.S.O.; Warren, J.E.; et al. Chemically blockable transformation and ultraselective low-pressure gas adsorption in a non-porous metal organic framework. *Nat. Chem.* **2009**, *1*, 289–294. [CrossRef] [PubMed]
3. Arai, H.; Machida, M. Removal of NOx through sorption-desorption cycles over metal oxides and zeolites. *Catal. Today* **1994**, *22*, 97–109. [CrossRef]
4. Cruz, W.V.; Leung, P.C.W.; Seff, K. Crystal structure of nitric oxide and nitrogen dioxide sorption complexes of partially cobalt(II)-exchanged zeolite A. *Inorg. Chem.* **1979**, *18*, 1692–1696. [CrossRef]
5. Zhang, J.; Kosaka, W.; Kitagawa, S.; Takata, M.; Miyasaka, H. In Situ Tracking of Dynamic NO Capture through a Crystal-to-Crystal Transformation from a Gate-Open-Type Chain Porous Coordination Polymer to a NO-Adducted Discrete Isomer. *Chem. Eur. J.* **2019**, *25*, 3020–3031. [CrossRef]
6. Zhang, W.-X.; Yahiro, H.; Iwamoto, M.; Izumi, J. Reversible and irreversible adsorption of nitrogen monoxide on cobalt lon-exchanged ZSM-5 and mordenite zeolites at 273–523 K. *J. Chem. Soc. Faraday Trans.* **1995**, *91*, 767–771. [CrossRef]
7. Møller, M.S.; Haag, A.; McKee, V.; McKenzie, C.J. NO sorption, in-crystal nitrite and nitrate production with arylamine oxidation in gas-solid single crystal to single crystal reactions. *Chem. Commun.* **2019**, *55*, 10551–10554. [CrossRef]
8. Earnshaw, A.; Hewlett, P.C.; Larkworthy, L.F. 877. Transition metal–Schiff's base complexes. Part II. The reaction of nitric oxide with some oxygen-carrying cobalt compounds. *J. Chem. Soc.* **1965**, *0*, 4718–4723. [CrossRef]
9. Diehl, H.; Hach, C.C.; Harrison, G.C.; Liggett, L.M.; Chao, T.S. Studies on oxygen-carrying cobalt compounds; cobalt derivatives of the Schiff's bases of salicylaldehyde with alkylamines. *Iowa State Coll. J. Sci.* **1947**, *21*, 287.

10. Jacobsen, E.N.; Zhang, W.; Muci, A.R.; Ecker, J.R.; Deng, L. Highly enantioselective epoxidation catalysts derived from 1,2-diaminocyclohexane. *J. Am. Chem. Soc.* **1991**, *113*, 7063–7064. [CrossRef]
11. Lee, N.H.; Muci, A.R.; Jacobsen, E.N. Enantiomerically pure epoxychromans via asymmetric catalysis. *Tetrahedron Lett.* **1991**, *32*, 5055–5058. [CrossRef]
12. Hanson, J. Synthesis and use of jacobsen's catalyst: Enantioselective epoxidation in the introductory organic laboratory. *J. Chem. Educ.* **2001**, *78*, 1266. [CrossRef]
13. Groom, C.R.; Bruno, I.J.; Lightfoot, M.P.; Ward, S.C. The cambridge structural database. *Acta Crystallogr. B Struct. Sci. Cryst. Eng. Mater.* **2016**, *72*, 171–179. [CrossRef]
14. Møller, M.S.; Kongsted, J.; McKenzie, C.J. Preparation of organocobalt(iii) complexes via O_2 activation. *Dalton Trans.* **2021**, *50*, 4819–4829. [CrossRef] [PubMed]
15. Brückner, S.; Calligaris, M.; Nardin, G.; Randaccio, L. The crystal structure of the form of N,N′-ethylenebis(salicylaldehydeiminato) cobalt(II) inactive towards oxygenation. *Acta Crystallogr. B Struct. Crystallogr. Cryst. Chem.* **1969**, *25*, 1671–1674. [CrossRef]
16. Hughes, D.L.; Kleinkes, U.; Leigh, G.J.; Maiwald, M.; Sanders, J.R.; Sudbrake, C. New polymeric compounds containing vanadium–oxygen chains. *J. Chem. Soc. Dalton Trans.* **1994**, 2457–2466. [CrossRef]
17. Garcia-Deibe, A.; Sousa, A.; Bermejo, M.R.; Mac Rory, P.P.; McAuliffe, C.A.; Pritchard, R.G.; Helliwell, M. The visible light induced rearrangement of a manganese(III) complex of an unsymmetrical tetradentate Schiff's base ligand, 4-[2-(2-hydroxyphenylmethyleneamino)ethylamino]pent-3-en-2-one, to a manganese(III) complex of the symmetrical ligand salen. *J. Chem. Soc. Chem. Commun.* **1991**, *10*, 728–729. [CrossRef]
18. Bhadbhade, M.M.; Srinivas, D. Effects on molecular association, chelate conformation, and reactivity toward substitution in copper Cu(5-X-salen) complexes, salen2- = N,N′-ethylenebis(salicylidenaminato), X = H, CH3O, and Cl: Synthesis, x-ray structures, and EPR investigations. [Erratum to document cited in CA119(26):285036b]. *Inorg. Chem.* **1993**, *32*, 6122–6130.
19. *CrysAlis*, version 1.171.40.67a; Rigaku Oxford Diffraction: The Woodlands, TX, USA, 2019.
20. Hübschle, C.B.; Sheldrick, G.M.; Dittrich, B. ShelXle: A Qt graphical user interface for SHELXL. *J. Appl. Crystallogr.* **2011**, *44*, 1281–1284. [CrossRef]
21. Sheldrick, G.M. SHELXT—Integrated space-group and crystal-structure determination. *Acta Crystallogr. A Found. Adv.* **2015**, *71*, 3–8. [CrossRef]
22. Sheldrick, G.M. Crystal structure refinement with SHELXL. *Acta Crystallogr. C Struct. Chem.* **2015**, *71*, 3–8. [CrossRef]
23. Bochevarov, A.D.; Harder, E.; Hughes, T.F.; Greenwood, J.R.; Braden, D.A.; Philipp, D.M.; Rinaldo, D.; Halls, M.D.; Zhang, J.; Friesner, R.A. Jaguar: A high-performance quantum chemistry software program with strengths in life and materials sciences. *Int. J. Quantum Chem.* **2013**, *113*, 2110–2142. [CrossRef]
24. *Jaguar*; Schrödinger Release 2019-1; Schrödinger, LLC: New York, NY, USA, 2019.
25. Hay, P.J.; Wadt, W.R. Ab initio effective core potentials for molecular calculations. Potentials for K to Au including the outermost core orbitals. *J. Chem. Phys.* **1985**, *82*, 299–310. [CrossRef]
26. Stephens, P.J.; Devlin, F.J.; Chabalowski, C.F.; Frisch, M.J. Ab Initio Calculation of Vibrational Absorption and Circular Dichroism Spectra Using Density Functional Force Fields. *J. Phys. Chem.* **1994**, *98*, 11623–11627. [CrossRef]
27. Banks, J.L.; Beard, H.S.; Cao, Y.; Cho, A.E.; Damm, W.; Farid, R.; Felts, A.K.; Halgren, T.A.; Mainz, D.T.; Maple, J.R.; et al. Integrated modeling program, applied chemical theory (IMPACT). *J. Comput. Chem.* **2005**, *26*, 1752–1780. [CrossRef] [PubMed]
28. Larrow, J.F.; Jacobsen, E.N. (R,R)-N,N′-Bis(3,5-di-tert-butylsalicylidene)-1,2-cyclohexanediamino manganese(III) chloride, a highly enantioselective epoxidation catalyst. *Org. Synth.* **1998**, *75*, 1.
29. Li, G.; Liu, Y.; Zhang, K.; Shi, J.; Wan, X.; Cao, S. Effect of salen-metal complexes on thermosensitive reversibility of stimuli-responsive water-soluble poly(urethane amine)s. *J. Appl. Polym. Sci.* **2013**, *129*, 3696–3703. [CrossRef]
30. North, M.; Quek, S.C.Z.; Pridmore, N.E.; Whitwood, A.C.; Wu, X. Aluminum(salen) complexes as catalysts for the kinetic resolution of terminal epoxides via co$_2$ coupling. *ACS Catal.* **2015**, *5*, 3398–3402. [CrossRef]
31. Xu, N.; Powell, D.R.; Cheng, L.; Richter-Addo, G.B. The first structurally characterized nitrosyl heme thiolate model complex. *Chem. Commun.* **2006**, *19*, 2030–2032. [CrossRef] [PubMed]
32. Xu, N.; Powell, D.R.; Richter-Addo, G.B. Nitrosylation in a crystal: Remarkable movements of iron porphyrins upon binding of nitric oxide. *Angew. Chem. Int. Ed. Engl.* **2011**, *50*, 9694–9696. [CrossRef] [PubMed]
33. Parsons, S.; Flack, H.D.; Wagner, T. Use of intensity quotients and differences in absolute structure refinement. *Acta Crystallogr. B Struct. Sci. Cryst. Eng. Mater.* **2013**, *69*, 249–259. [CrossRef]
34. Haller, K.J.; Enemark, J.H. Structural chemistry of the {CoNO}^{8} group. III. The structure of *N*, *N*′-ethylenebis(salicylideneiminato) nitrosylcobalt(II), Co(NO)(salen). *Acta Crystallogr. B Struct. Sci.* **1978**, *34*, 102–109. [CrossRef]
35. Enemark, J.H.; Feltham, R.D. Principles of structure, bonding, and reactivity for metal nitrosyl complexes. *Coord. Chem. Rev.* **1974**, *13*, 339–406. [CrossRef]
36. Albrecht, E.; Baum, G.; Bellunato, T.; Bressan, A.; Dalla Torre, S.; D'Ambrosio, C.; Davenport, M.; Dragicevic, M.; Duarte Pinto, S.; Fauland, P.; et al. VUV absorbing vapours in n-perfluorocarbons. *Nucl. Instrum. Methods Phys. Res. A Accel. Spectrometers Detect. Assoc. Equip.* **2003**, *510*, 262–272. [CrossRef]
37. Nafie, L.A. *Vibrational Optical Activity: Principles and Applications*; John Wiley & Sons, Ltd.: Chichester, UK, 2011.

38. Bormett, R.W.; Asher, S.A.; Larkin, P.J.; Gustafson, W.G.; Ragunathan, N.; Freedman, T.B.; Nafie, L.A.; Balasubramanian, S.; Boxer, S.G. Selective examination of heme protein azide ligand-distal globin interactions by vibrational circular dichroism. *J. Am. Chem. Soc.* **1992**, *114*, 6864–6867. [CrossRef]
39. Adão, P.; Costa Pessoa, J.; Henriques, R.T.; Kuznetsov, M.L.; Avecilla, F.; Maurya, M.R.; Kumar, U.; Correia, I. Synthesis, characterization, and application of vanadium-salan complexes in oxygen transfer reactions. *Inorg. Chem.* **2009**, *48*, 3542–3561. [CrossRef]
40. Chen, B.-L.; Zhu, H.-W.; Xiao, Y.; Sun, Q.-L.; Wang, H.; Lu, J.-X. Asymmetric electrocarboxylation of 1-phenylethyl chloride catalyzed by electrogenerated chiral [CoI(salen)]−complex. *Electrochem. Commun.* **2014**, *42*, 55–59. [CrossRef]
41. Bam, R.; Pollatos, A.S.; Moser, A.J.; West, J.G. Mild olefin formation via bio-inspired vitamin B_{12} photocatalysis. *Chem. Sci.* **2021**, *12*, 1736–1744. [CrossRef]
42. Chang, S.; Lee, N.H.; Jacobsen, E.N. Regio- and enantioselective catalytic epoxidation of conjugated polyenes. Formal synthesis of LTA4 methyl ester. *J. Org. Chem.* **1993**, *58*, 6939–6941. [CrossRef]
43. Huang, J.; Cai, J.; Feng, H.; Liu, Z.; Fu, X.; Miao, Q. Synthesis of salen Mn(III) immobilized onto the ZnPS-PVPA modified by 1,2,3-triazole and their application for asymmetric epoxidation of olefins. *Tetrahedron* **2013**, *69*, 5460–5467. [CrossRef]
44. Buhse, T.; Cruz, J.-M.; Noble-Terán, M.E.; Hochberg, D.; Ribó, J.M.; Crusats, J.; Micheau, J.-C. Spontaneous Deracemizations. *Chem. Rev.* **2021**, *121*, 2147–2229. [CrossRef] [PubMed]